Applied Surface Science 349 (2015) 576–581

Contents lists available at ScienceDirect

Applied Surface Science

journal homepage: www.elsevier.com/locate/apsusc

Influence of substrate on nucleation and growth of vertical graphene nanosheets

Subrata Ghosh*, K. Ganesan*, S.R. Polaki, Tom Mathews, Sandip Dhara, M. Kamruddin, A.K. Tyagi

Surface and Nanoscience Division, Materials Science Group, Indira Gandhi Centre for Atomic Research, Kalpakkam 603102, India

ARTICLE INFO

Article history:
Received 20 April 2015
Received in revised form 6 May 2015
Accepted 7 May 2015
Available online 15 May 2015

Keywords:
Vertical graphene nanosheets
ECR-CVD
Raman spectroscopy
SEM
Nucleation

ABSTRACT

The present study reports the role of substrate on nucleation and growth of vertical graphene nanosheets (VGNs) under electron cyclotron resonance chemical vapor deposition (ECR-CVD). The VGNs are grown on Pt, Ni, Au, Cu, Si(100), Si(111), SiO_2 and quartz substrates simultaneously. The morphology of VGNs is found to vary significantly with substrate. VGNs on Pt have the highest aerial density of vertical sheets while quartz have the lowest. The structural defects in VGNs vary with substrate as evidenced from Raman spectroscopy. The observation of defect related Raman bands such as D″ and D* at 1150 and 1500 cm^{-1}, respectively revealed the existence of pentagon–heptagon rings or carbon onions in VGNs. Formation of such defects at early stage of nucleation dictates the growth mechanism and hence the morphology. A phenomenological four-stage model is discussed, to substantiate the nucleation and growth mechanism of VGNs on different substrates, by evoking substrate–plasma interaction during growth.

1. Introduction

The vertical graphene nanosheets (VGNs), one of the remarkable nanostructures in nanocarbon family, has attracted considerable attention of academic and industrial research due to their unique structural, electrical, optical and mechanical properties [1,2]. The VGNs, also known as carbon nanowalls (CNWs), contain open edge interconnected three-dimensional networks of vertically aligned graphene nanosheets which are freely standing perpendicular to the substrates [2,3]. Each sheet is composed of a few layers of graphene with length and height ranging from a few nanometers to microns. The inherent large surface area, high conductivity, capability for easy functionalization and sharp edges make them very attractive for field emission, chemical- and bio-sensors and energy storage devices [2,4].

Plasma enhanced chemical vapor deposition (PECVD) is one of the most capable and preferred techniques to grow VGNs. Earlier studies on growth of carbon nanotubes by plasma based techniques using metallic catalyst lead to the invention of VGNs [2]. Subsequently, a large volume of research had been carried out to control the morphology, growth rates and structural properties of VGNs by varying the feedstock gas composition, microwave power, electric field, temperature and pressure [4–6]. The research on growth process of VGNs is also continued on different types of substrates viz. Si, SiO_2, Al_2O_3, MgO, quartz, Al, stainless steel, Pt, Ti, Cu, Ni, Mo, Zr, Hf, Nb, W, and Ta till date [2,7–12]. However, a little attention has been paid to understand the role of substrates on the growth mechanism of VGNs.

Hiramatsu et al. [8] found that the growth rate of VGNs on Ti to be 1.6 times more than that on Si, under identical growth conditions. Formation of interfacial carbide layer is reported to enhance the adhesion of VGNs on quartz and Si substrates [7]. The types of defects in VGNs are also found to depend on substrates, which can be attributed to variation in their hydrocarbon species adsorption ability [12]. The substrate properties such as thermal conductivity [7,9], electronic conductivity [13], surface roughness, lattice parameter, ability to adsorb hydrocarbon species [14] and plasma-surface interaction [15] are found to influence the nucleation and growth. From the results of the studies carried out by various research groups, it can be inferred that substrate plays indeed a crucial role in growth of VGNs. On contrary, a few groups have reported that the nucleation and growth of VGNs is substrate independent in PECVD [10,11]. Though the substrate surface effect on the VGNs growth is reported, the study on substrate dependent growth mechanism is scarce. Hence, a detailed analysis on the role of substrates is essential to understand the nucleation, growth rate and morphology of VGNs.

* Corresponding authors.
E-mail addresses: subrataghosh.phys@gmail.com, subrata@igcar.gov.in (S. Ghosh), kganesan@igcar.gov.in (K. Ganesan).

http://dx.doi.org/10.1016/j.apsusc.2015.05.038
0169-4332/

In view of the above, a detailed study on the growth of VGNs on different substrates is carried out using electron cyclotron resonance chemical vapor deposition (ECR-CVD). The substrate dependent morphology, growth rate and structural properties are investigated using field emission scanning electron microscopy (FESEM) and Raman spectroscopy, respectively. In order to find the role of substrates on nucleation, the surface of substrates is analyzed with water contact angle (WCA) measurements and atomic force microscopy (AFM). Further, early stage nucleation is correlated with substrate characteristics such as thermal conductivity, surface energy and its interaction with plasma using a phenomenological model. According to this model, the formation of localized nanoscale hot spot, due to substrate-plasma interaction, and substrate-hydrocarbon sticking co-efficient dictates the morphology and structural properties of VGNs.

2. Experimental methods

2.1. Growth of VGNs by ECR-CVD

The synthesis of VGNs on different substrates is performed simultaneously under 5 sccm of CH_4 (5 N purity) and 25 sccm of Ar (3 N purity) by ECR-CVD. The detail of the deposition system is reported elsewhere [12]. Different types of substrates from metallic to insulators, such as Pt, Ni, Au/Si(100), Cu, Si ((111) and (100)), SiO_2 and quartz are chosen for this study. Pt, Cu and Ni foils of thickness of 125 μm are used as metallic substrates (99.9% purity). A thin film of Au having thickness of about 165 nm is deposited on *n*-Si(100) by DC magnetron sputtering. SiO_2 of thickness 400 nm on *n*-Si(100) is prepared by thermal oxidation. To maintain identical growth conditions, all the substrates need to be placed within a homogeneous plasma field. This is ensured by growing VGNs over a large area (50 mm diameter). There is no change in morphology and structural quality across this area. Before loading into the chamber, the substrates are cleaned by wet chemical process. Prior to growth, the chamber is evacuated down to a base pressure of 5×10^{-6} mbar by a turbomolecular pump, the substrates are heated to 800 °C at a heating rate of 30 °C/min and retained for 30 min. Subsequently, the substrates are pre-cleaned by Ar plasma under 20 sccm flow for 10 min at 200 W microwave (MW) power. Thereafter, CH_4 is fed into the chamber through downstream injection ring along with Ar gas for 30 min at 400 W MW power, while maintaining the substrate temperature at 800 °C. After the growth, the plasma is turned off and the samples are annealed at the growth temperature for 30 min. The samples are then cooled down naturally to room temperature.

2.2. Characterization

Morphological features of the films are observed by FESEM (Supra 55, Zeiss). The structural properties, in terms of defects and disorder, are evaluated by micro-Raman spectroscopy (Renishaw inVia, UK) with 514.5 nm laser and 100× objective lens. A 1800 gr/mm grating is used for the mono-chromatization of scattered signal and a thermoelectric cooled CCD detector is used for the Raman studies in backscattering configuration. In order to avoid the laser induced heating of the sample, the laser power is kept below 1 mW. The Raman spectra of the film are fitted with Lorentzian line shape using WIRE 3.2 software. The water contact angle (WCA) of the surfaces is measured by sessile drop method with the help of a CCD camera (Holmarc, HO-IAD-CAM-01, India). The volume of the water droplet is about 1 μl. The root mean square (rms) roughness of substrate surfaces is measured by a commercial AFM.

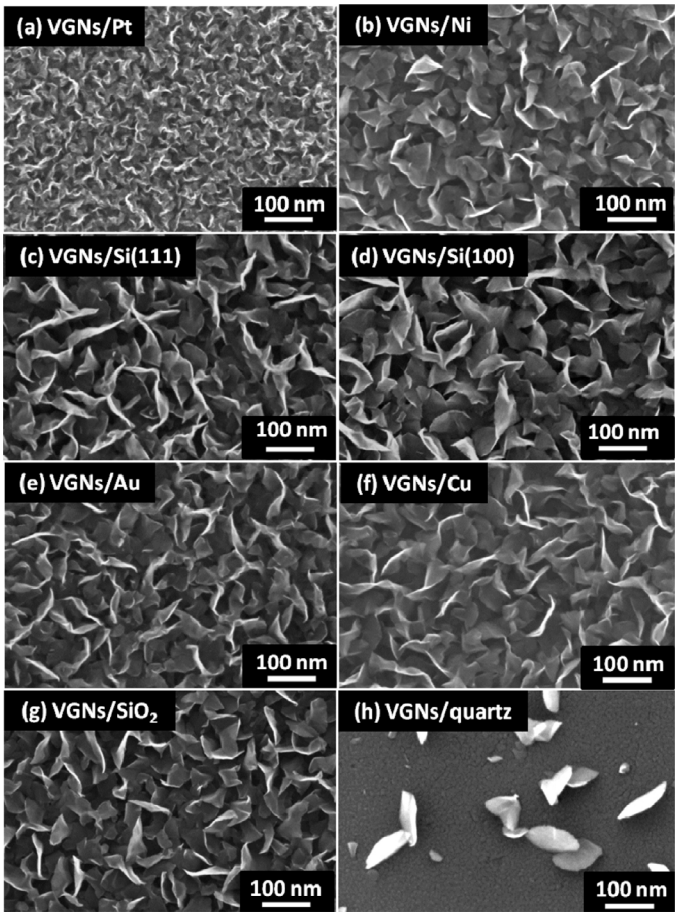

Fig. 1. SEM images of VGNs grown on (a) Pt, (b) Ni, (c) *n*-Si(111), (d) *n*-Si(100), (e) Au/Si, (f) Cu, (g) SiO_2, and (h) quartz substrates.

3. Results

3.1. Morphology analysis

The morphology of VGNs grown simultaneously over different substrates is depicted in Fig. 1. The as-grown VGNs are homogeneous, uniform and densely packed, except those grown on quartz. However, a discernable variation in morphology is observed for the VGNs grown on different substrates. The morphology of VGNs grown on Pt is found to be maze-like, whereas it is petal-like on all other substrates. The cross sectional height of VGNs on different substrates varies from 169 to 264 nm. The aerial density of VGNs is found to be highest for Pt and lowest for quartz substrates. The difference in height and aerial density of VGNs grown on these substrates indicates that the nucleation and growth rate are different on different substrates. The difference in height of VGNs grown on Si(111) and Si(100) indicates the anisotropic nature of the growth.

3.2. Surface analysis

Wetting study is one of the basic characterization tools to provide information about surface energy, chemical reactivity and wettability of a surface. Hence, to get more insight into the differential growth of VGNs, the substrate surface roughness and wetting properties are studied using AFM topography and WCA measurements, respectively. The Table 1 shows WCA values measured over the substrate surfaces, which had undergone all pre-cleaning treatment, before and after VGNs growth. A representative image, depicting WCA before and after growth of VGNs on Si(100), is

Table 1
The extracted parameter of contact angle measurement of different surfaces before and after growth of VGNs, rms roughness of pre-cleaned substrates and their respective thermal conductivity from literature.

Substrates	Contact angle (°)		Thermal conductivity (W/m K)	r.m.s. value (nm)
	Before growth	After growth		
Pt	62.9 ± 3.2	121.9 ± 0.9	71.9 [16]	2.0 ± 0.5
Ni	71.7 ± 4.1	123.1 ± 2.8	93 [16]	2.5 ± 1.9
Si(100)	72.8 ± 0.7	135.2 ± 0.9	133 [17]	0.4 ± 0.1
Si(111)	76.5 ± 1.4	133.7 ± 0.1	156 [18]	0.4 ± 0.1
Au	85.5 ± 0.6	134.0 ± 0.3	318 [16]	2.3 ± 0.8
Cu	101.4 ± 3.9	136.6 ± 0.2	402 [16]	3.6 ± 0.8
SiO_2	79.1 ± 2.4	131.6 ± 0.2	1.29 [17]	0.4 ± 0.1
Quartz	75.3 ± 0.8	105.9 ± 3.7	1.5–3	0.5 ± 0.1

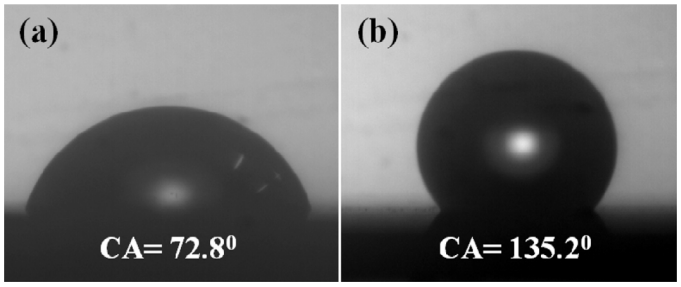

Fig. 2. Water contact angle of Si(100) (a) before growth and (b) after growth of VGNs.

shown in Fig. 2. The pre-cleaned substrates exhibit WCA less than 90° except for Cu indicating the hydrophilic nature of substrates. The Pt has the lowest WCA of 62.9° and Cu has the highest WCA of 101.4°. The variation in WCA can be attributed to the different surface energies of substrates.

After the growth of VGNs, the surface transforms from hydrophilic to hydrophobic. The VGNs on Cu exhibit the highest hydrophobic behavior with WCA of 136.6 ± 0.2° while quartz shows the least hydrophobicity with WCA of 105.9 ± 3.7°. The difference in WCA can be attributed to the variation in aerial density of VGNs on the substrate. From the FESEM micrographs, it is clear that aerial density of VGNs on quartz is the least and it has the lowest WCA. The lower WCA signifies higher surface energy. Note that, the surface energy of substrates can strongly influence the early stage nucleation of adatoms during thin film growth.

A clear trend in aerial density of VGNs with surface energy can be discerned from the FESEM images, except in the case of quartz. The VGNs on Pt with the highest surface energy has the highest aerial density followed by Ni. The variation in aerial density is not much in the case of other substrates. The anomaly of VGNs on quartz may be due to other substrate properties than surface energy. Surface energy is one of the factors affecting the nucleation density and hence growth of VGNs with different morphology on various substrates. The rms roughness measured over 1 μm × 1 μm area on different substrates is given in Table 1. However, there is no significant correlation between roughness of pre-treated substrates and morphology of VGNs.

3.3. Raman analysis

The Raman spectroscopy is a well established technique to probe structural, electronic and phonon properties of carbon nanostructures. It is a very sensitive technique for investigating structural defects and disorder in the structure. The Raman spectra of VGNs grown on different substrates seem nearly similar, as shown in Fig. 3(a). The G- and G′-bands confirm the graphitic structure. The defect related bands (D-, D′-, D + D′ and 2D′) are the result of defects and disorder due to large amount of edge states, nanographitic (NG) base layer with sp^3 bonded C–H species and ion-induced defects from the plasma during growth. The spectra consist of prominent D-, G-, and G′-bands which are characteristics of VGNs [12,19]. The observed large defects in VGNs are due to the presence of disorder, which arises from large amount of edge states, sp^3 bonded C–H species, NG base layer, point defects and ion-induced defects from the plasma during growth.

The extracted parameters show differences in structural characteristics of VGNs as listed in Table 2. As shown in Fig. 3(a), the G and D′ bands almost overlap for VGNs grown on Pt which indicates higher amount of defects. It is consistent with the observation made in the morphological studies (Fig. 1) that VGNs on Pt substrate have higher edge density, more crumpled maze-like structure with higher sheet curvature. Similarly, the FWHM of D-, G- and G′-bands of VGNs on Pt is also higher than on other substrates indicating the higher defects on Pt (Table 2). The lowest FWHM of G-band (33.1 cm^{-1}) is found for VGNs grown on quartz which is consistent with the earlier report [12]. Further, the position of the G-band on Pt is about 1589 cm^{-1} and for all other substrates it is around 1585 cm^{-1}. Such variation in G-band position could be due to different levels of strain in VGNs grown on different substrates [20]. The lattice mismatch between substrate and interfacial NG base layer or defects present can induce such strain [3]. Also, it is known that the intensity ratios of D to G (I_D/I_G) provide a measure of defects/disorder in a disordered graphitic system. The crystalline sizes (L_a) of nanographitic domain are calculated using the Tuinstra-Koeing relation [21].

$$L_a = C(\lambda)\left(\frac{I_D}{I_G}\right)^{-1} \quad (1)$$

where $C(\lambda = 514.5\ nm) = 4.4$ nm. It is found that the crystalline size of VGNs varies from 1.64 to 2.08 nm depending on the substrates, as given in Table 2. Thus, the variation of parameters extracted from Raman spectra of VGNs grown on different substrates is due to the variation in aerial density and degree of graphitization.

Furthermore, a closer view of Raman spectra shows that the valley between D and G bands is upshifted as shown in Fig. 3(b). The best fit for the first order Raman spectra is found to have two additional bands at about 1140 and 1500 cm^{-1} in addition to prominent D, G and D′ bands. The peak at about 1140 cm^{-1} is assigned as D″-band [12,19], which can arise due to high density of edges [22], bond stretching mode of sp^3 hydrogenated carbon [23] and presence of pentagon rings [24]. The peak at about 1500 cm^{-1} is assigned as D* band which is attributed to the presence of interstitial defects or out-of-plane defects [25], pentagon–heptogon structure [24], trans-polyethylene [26] and fullerene-like structures [27].

4. Discussion

As discussed earlier, FESEM analysis confirms that the aerial density, vertical height and shape of nanosheets (petal-like or maze-like) are found to vary with respect to substrate (Fig. 1).

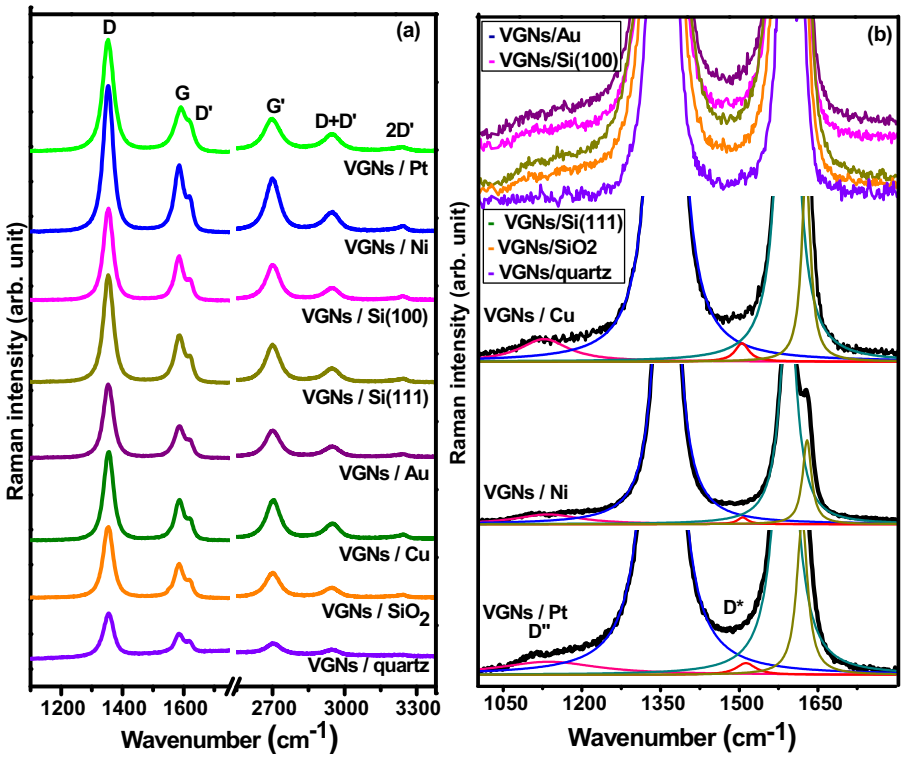

Fig. 3. (a) Raman spectra and (b) zoomed area of first order Raman spectra of VGNs grown on various substrates.

Table 2
The extracted parameters of Raman spectra of VGNs grown on different substrates.

Substrate	Pos_D (cm^{-1})	$FWHM_D$ (cm^{-1})	Pos_G (cm^{-1})	$FWHM_G$ (cm^{-1})	$Pos_{G'}$ (cm^{-1})	$FWHM_{G'}$ (cm^{-1})	I_D/I_G	L_a (nm)
Pt	1353.3 ± 0.4	43.3 ± 0.5	1589.1 ± 0.2	46.7 ± 0.5	2698.0 ± 0.7	85.7 ± 2.4	2.68	1.64
Ni	1353.8 ± 0.0	37.3 ± 0.2	1585.0 ± 0.1	36.5 ± 0.1	2700.5 ± 0.1	69.1 ± 0.2	2.23	1.97
n-Si(100)	1353.7 ± 0.4	36.9 ± 0.2	1584.5 ± 0.3	34.9 ± 0.7	2701.3 ± 0.4	68.5 ± 0.6	2.12	2.08
n-Si(111)	1353.7 ± 0.1	38.5 ± 0.2	1585.6 ± 0.0	39.4 ± 0.1	2700.0 ± 0.1	72.9 ± 0.9	2.23	1.95
Au/Si	1353.7 ± 0.3	39.1 ± 0.3	1585.5 ± 0.0	39.8 ± 0.3	2699.9 ± 0.2	73.5 ± 0.7	2.34	1.88
Cu	1354.8 ± 0.4	37.8 ± 0.0	1585.9 ± 0.4	36.9 ± 0.1	2702.4 ± 0.4	70.3 ± 1.0	2.21	1.99
SiO_2	1353.3 ± 0.2	38.3 ± 0.2	1585.0 ± 0.3	35.8 ± 0.2	2700.5 ± 0.1	71.0 ± 0.5	2.15	2.05
Quartz	1355.1 ± 0.4	38.7 ± 0.2	1585.5 ± 0.3	33.1 ± 0.4	2703.8 ± 0.7	70.5 ± 1.8	2.37	1.86

Further, the height of VGNs and WCA measured on these substrates increase with thermal conductivity of the substrates as given in Table 1 except for SiO_2 and quartz substrates. Thus, in addition to the surface energy, thermal conductivity of substrates influence early stage nucleation of VGNs.

Fig. 4 shows the graphical representation of nucleation and growth mechanism of VGNs on various substrates. At first, during pre-cleaning process, the Ar plasma removes surface contaminations and creates localized hot spots [28] on substrate surface (Fig. 4(a)). These localized hot spots are the energetically most favorable regions to adsorb the hydrocarbon species. The power balance at substrate surface during its interaction with plasma can be described as follows [29]. The input power or total flux of heat towards substrate is

$$\dot{Q}_{in} = \left[\varrho_S d_S A_S c_S \left(\frac{dT_S}{dt}\right)\right] + \left[\alpha\chi p T_S A_S + \frac{\lambda_S}{d_S} A_S (T_S - T_H) + 2\sigma A_S (T_S - T_H)\right] \quad (2)$$

In Eq. (2), the first and second terms represent the transferred power to heat the substrate and the liberated power from the substrate respectively. The ϱ_S, d_S, A_S, c_S, and λ_S are mass density, thickness, area, specific heat capacity, thermal conductivity, respectively. The α is the sticking co-efficient of plasma species on the substrate surface, χ is the molecular heat conductivity of gas, p the gas pressure (10^{-3} mbar, here) and σ the Stefan–Boltzmann

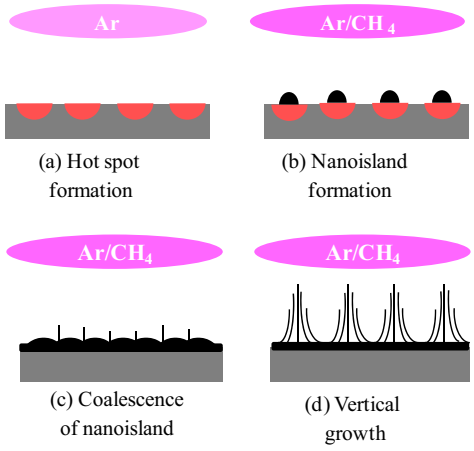

Fig. 4. Schematic representation of four stages of growth of VGNs under plasma.

co-efficient. In the case of PECVD growth, the substrate surface temperature (T_S) is always greater than the heater temperature (T_H), the due to plasma surface interaction. Hence, the size and density of such localized hot spots depend on the substrate and plasma characteristics.

At second stage, when CH_4 is fed into the growth chamber, MW energy in ECR-CVD creates a high density plasma with a variety of free radicals such as CH_x, C_xH_y, C_2 dimers, Ar–H, atomic hydrogen and in their several possible combinations [15]. The carbon and hydro-carbon radicals get adsorbed onto the hot spots due to surface diffusion, initiating rapid nucleation of NG islands. The adsorption rate or sticking co-efficient (α) of radicals depends on the nature of the substrate [30], localized hot spot size and plasma process parameters (χ, p, T_S, T_H). Thus the size, shape and density of NG islands depend on the characteristics of localized hot spots (Fig. 4(b)).

In third stage (Fig. 4(c)), the NG islands coalesce and form interfacial NG base layer over the substrates. The interfacial base layer contains highly defective NG, amorphous carbon (*a-C*), carbon onions and point defects such as pentagon, heptagon rings. Raman analysis confirmed the presence of such defects from the observation of D″ and D* in the first order Raman spectra (Fig. 3). Direct evidence of the defects viz. *a-C* and carbon onions are shown by Zhao et al. [3] using transmission electron microscopy.

In final stage, the coalescence of nanoislands and growth causes stress at NG grain boundaries, whose release favors nucleation and further growth of graphene nanosheets in the vertical direction [31]. The nucleation of vertical growth could start either from the defective NG buffer layer or from the surface carbon onions [3]. The vertical growth is found to be influenced by the in-built electric field associated with the plasma [32]. Further, the plasma produces a relatively higher temperature and chemical potential gradients near the substrate surface enhancing the vertical growth (Fig. 4(d)) [3,15].

It is noteworthy that the morphology of VGNs on SiO_2 and quartz are entirely different even though both substrates have similar thermal conductivity, rms roughness and are amorphous in nature (Table 1). This is because thermally oxidized Si (SiO_2) contains large amount of defects which act as nucleation sites resulting in high density of VGNs. Whereas quartz substrates with relatively less defects produce VGNs of low density. Further investigation is required to understand the nucleation of VGNs on SiO_2 and quartz substrates.

Overall, we note that the physical characteristics of NG interfacial layer play a crucial role in determining the growth rate, morphology and structure of VGNs grown on different substrates. The physical characteristics of NG base layer depend on the surface energy and thermal conductivity of substrates. A larger amount of hot spots are formed when the thermal conductivity/surface energy of the substrate is low/high and hence higher aerial density and vice versa.

5. Conclusion

The vertical graphene nanosheets (VGNs) are grown on different substrates simultaneously under identical conditions using electron cyclotron resonance chemical vapor deposition (ECR-CVD) technique. The morphology (maze-like and petal-like), growth rates and degree of graphitization of VGNs are found to be substrate dependant. The growth mechanism of VGNs on various substrates is explained with a phenomenological model invoking substrate–plasma interaction. During substrate–plasma interaction, a high density of localized hot spots are created which serve as nucleation centers for nanographitic (NG) island formation. The formation of interfacial NG layer by NG island coalescence is the key factor for VGNs growth and it varies with substrate. Thus, the substrates guide the growth of VGNs through the interfacial NG layer. This study is an effort to provide improved understanding of VGNs growth on different substrates and also helps to choose substrates to grow VGNs with desired characteristics.

References

[1] Z. Bo, S. Mao, Z. Jun Han, K. Cen, J. Chen, K. Ostrikov, Emerging energy and environmental applications of vertically-oriented graphenes, Chem. Soc. Rev. 44 (2015) 2018–2121.
[2] Y. Wu, P. Qiao, T. Chong, Z. Shen, Carbon nanowalls grown by microwave plasma enhanced chemical vapor deposition, Adv. Mater. 14 (2002) 64–67.
[3] J. Zhao, M. Shaygan, J. Eckert, M. Meyyappan, M.H. Rümmeli, A growth mechanism for free-standing vertical graphene, Nano Lett. 14 (2014) 3064–3071.
[4] M. Hiramatsu, M. Hori, Fabrication of carbon nanowalls using novel plasma processing, Jpn. J. Appl. Phys. 45 (2006) 5522.
[5] K. Shiji, M. Hiramatsu, A. Enomoto, M. Nakamura, H. Amano, M. Hori, Vertical growth of carbon nanowalls using rf plasma-enhanced chemical vapor deposition, Diamond Relat. Mater. 14 (2005) 831–834.
[6] S. Suzuki, A. Chatterjee, C.-L. Cheng, M. Yoshimura, Effect of hydrogen on carbon nanowall growth by microwave plasma-enhanced chemical vapor deposition, Jpn. J. Appl. Phys. 50 (2011) 01AF08.
[7] R. Vitchev, A. Malesevic, R.H. Petrov, R. Kemps, M. Mertens, A. Vanhulsel, C. Van Haesendonck, Initial stages of few-layer graphene growth by microwave plasma-enhanced chemical vapour deposition, Nanotechnology 21 (2010) 095602.
[8] M. Hiramatsu, Y. Nihashi, H. Kondo, M. Hori, Nucleation control of carbon nanowalls using inductively coupled plasma-enhanced chemical vapor deposition, Jpn. J. Appl. Phys., 52 (2013) 01AK05.
[9] S.Y. Kim, Y.H. Joung, W.S. Choi, Growth properties of carbon nanowalls on glass substrates by a microwave plasma-enhanced chemical vapor deposition, Jpn. J. Appl. Phys. 53 (2014) 05FD09.
[10] J. Wang, M. Zhu, R.A. Outlaw, X. Zhao, D.M. Manos, B.C. Holloway, Synthesis of carbon nanosheets by inductively coupled radio-frequency plasma enhanced chemical vapor deposition, Carbon 42 (2004) 2867–2872.
[11] M. Hiramatsu, K. Shiji, H. Amano, M. Hori, Fabrication of vertically aligned carbon nanowalls using capacitively coupled plasma-enhanced chemical vapor deposition assisted by hydrogen radical injection, Appl. Phys. Lett. 84 (2004) 4708–4710.
[12] S. Ghosh, K. Ganesan, S.R. Polaki, T. Ravindran, N.G. Krishna, M. Kamruddin, A. Tyagi, Evolution and defect analysis of vertical graphene nanosheets, J. Raman Spectrosc. 45 (2014) 642–649.
[13] Z. Wang, M. Shoji, H. Ogata, Fabrication and electrochemical characterization of carbon nanosheets by microwave plasma-enhanced chemical vapor deposition, Jpn. J. Appl. Phys. 51 (2012) 01AH02.
[14] L. Zhang, Z. Shi, Y. Wang, R. Yang, D. Shi, G. Zhang, Catalyst-free growth of nanographene films on various substrates, Nano Res. 4 (2011) 315–321.
[15] K. Ostrikov, E. Neyts, M. Meyyappan, Plasma nanoscience: from nano-solids in plasmas to nano-plasmas in solids, Adv. Phys. 62 (2013) 113–224.
[16] C. Uher, Thermal conductivity of metals, in: Thermal Conductivity, Springer, 2004, pp. 21–91.
[17] J.H. Kim, A. Feldman, D. Novotny, Application of the three omega thermal conductivity measurement method to a film on a substrate of finite thickness, J. Appl. Phys. 86 (1999) 3959–3963.
[18] C. Glassbrenner, G.A. Slack, Thermal conductivity of silicon and germanium from 3 K to the melting point, Phys. Rev. 134 (1964) A1058.
[19] A.C. Ferrari, D.M. Basko, Raman spectroscopy as a versatile tool for studying the properties of graphene, Nat. Nanotechnol. 8 (2013) 235–246.
[20] Y.y. Wang, Z.h. Ni, T. Yu, Z.X., Shen, H.m. Wang, Y.h. Wu, W. Chen, A.T. Shen Wee, Raman studies of monolayer graphene: the substrate effect, J. Phys. Chem. C 112 (2008) 10637–10640.
[21] F. Tuinstra, J.L. Koenig, Raman spectrum of graphite, J. Chem. Phys. 53 (1970) 1126–1130.
[22] J. Wang, M. Zhu, R. Outlaw, X. Zhao, D. Manos, B. Holloway, V. Mammana, Free-standing subnanometer graphite sheets, Appl. Phys. Lett. 85 (2004) 1265–1267.
[23] S. Karlin, Ph. Colomban, Raman study of the chemical and thermal degradation of as-received and sol–gel embedded Nicalon and Hi-Nicalon SiC fibres used in ceramic matrix composites, J. Raman Spectrosc. 28 (1997) 219–228.
[24] R. Tarrant, D. McKenzie, M. Bilek, Raman characterisation of PIII multilayer carbon films, Diamond Relat. Mater. 13 (2004) 1422–1426.
[25] J. Rouzaud, A. Oberlin, C. Beny-Bassez, Carbon films: structure and microtexture (optical and electron microscopy, Raman spectroscopy), Thin Solid Films 105 (1983) 75–96.
[26] A.C. Ferrari, J. Robertson, Raman spectroscopy of amorphous, nanostructured, diamond-like carbon, and nanodiamond, Philos. Trans. R. Soc. Lond. A 362 (2004) 2477–2512.
[27] V. Blank, V. Denisov, A. Kirichenko, B. Kulnitskiy, S.Y. Martushov, B. Mavrin, I. Perezhogin, High pressure transformation of single-crystal graphite to form molecular carbon–onions, Nanotechnology 18 (2007) 345601.
[28] K.K. Ostrikov, I. Levchenko, U. Cvelbar, M. Sunkara, M. Mozetic, From nucleation to nanowires: a single-step process in reactive plasmas, Nanoscale 2 (2010) 2012–2027.

[29] H. Kersten, H. Deutsch, H. Steffen, G. Kroesen, R. Hippler, The energy balance at substrate surfaces during plasma processing, Vacuum 63 (2001) 385–431.
[30] M. Hori, T. Goto, Insights into sticking of radicals on surfaces for smart plasma nano-processing, Appl. Surf. Sci. 253 (2007) 6657–6671.
[31] A. Yoshimura, H. Yoshimura, S.C. Shin, K.-i. Kobayashi, M. Tanimura, M. Tachibana, Atomic force microscopy and Raman spectroscopy study of the early stages of carbon nanowall growth by dc plasma-enhanced chemical vapor deposition, Carbon 50 (2012) 2698–2702.
[32] M. Zhu, J. Wang, B.C. Holloway, R. Outlaw, X. Zhao, K. Hou, V. Shutthanandan, D.M. Manos, A mechanism for carbon nanosheet formation, Carbon 45 (2007) 2229–2234.